Dissociating thalamic alterations in Alcohol Use Disorder defines specificity of Korsakoff syndrome

Shailendra Segobin, Alice Laniepce, Ludivine Ritz, Coralie Lannuzel, Céline Boudehent, Nicolas Cabe, Laurent Urso, François Vabret, Francis Eustache, Helene Beaunieux, et al.

OXFORD UNIVERSITY PRESS | Brain

Dissociating thalamic alterations in Alcohol Use Disorder defines specificity of Korsakoff syndrome

Journal:	*Brain*
Manuscript ID	BRAIN-2018-01884.R1
Manuscript Type:	Original Article
Date Submitted by the Author:	n/a
Complete List of Authors:	Segobin, Shailendra; Inserm , U1077; Universite de Caen Basse-Normandie, UMR-S1077 Laniepce, Alice; Inserm , U1077; Universite de Caen Basse-Normandie, UMR-S1077 Ritz, Ludivine; Inserm U1077, ; Universite de Caen Basse-Normandie, UMR-S1077 Lannuzel, Coralie; Inserm U1077, Boudehent, Celine; Inserm U1077; Universite de Caen Basse-Normandie, UMR-S1077; Servide d'Addictologie, CHU Caen Cabe, NIcolas; Inserm , U1077; Servide d'Addictologie, CHU Caen; Universite de Caen Basse-Normandie, UMR-S1077 Urso, Laurent; Service d'Addictologie, Centre Hospitalier Roubaix Vabret, François; Inserm , U1077; Universite de Caen Basse-Normandie, UMR-S1077; Servide d'Addictologie, CHU Caen Eustache, Francis; INSERM, Université de Caen, EPHE, CHU de Caen, U1077 Beaunieux, Hélène; Inserm , U1077; Universite de Caen Basse-Normandie, UMR-S1077 Pitel, Anne Lise; Inserm , U1077; Universite de Caen Basse-Normandie, UMR-S1077
Subject category:	Neuropsychiatry
To search keyword list, use whole or part words followed by an *:	Memory < DEMENTIA, Tractography < DEMENTIA, Neurodegeneration: biomarkers < NEURODEGENERATION: CELLULAR AND MOLECULAR, Alcoholism < NEUROPSYCHIATRY, Neuropsychiatry: imaging < NEUROPSYCHIATRY, Neuropsychology < NEUROPSYCHIATRY

Dissociating thalamic alterations in Alcohol Use Disorder defines specificity of Korsakoff syndrome

Shailendra Segobin[1], PhD., Alice Laniepce[1], MSc., Ludivine Ritz[1], PhD., Coralie Lannuzel[1], MSc., Céline Boudehent[1,2],MSc., Nicolas Cabé[1,2], M.D., Laurent Urso[3], M.D., François Vabret[1,2], M.D., Francis Eustache[1], PhD., Hélène Beaunieux[1], PhD., Anne-Lise Pitel[1],PhD.

(1) Normandie Univ, UNICAEN, PSL Research University, EPHE, INSERM, U1077, CHU de Caen, Neuropsychologie et Imagerie de la Mémoire Humaine, 14000 Caen, France
(2) Service d'Addictologie, Centre Hospitalier Universitaire de Caen, 14000 Caen, France.
(3) Service d'Addictologie, Centre Hospitalier Roubaix, 59056 Roubaix, France.

Running title: Thalamic alterations in alcoholism

Keywords: Korsakoff's syndrome, diffusion tensor imaging, segmentation, anterior thalamic nuclei, mediodorsal thalamic nuclei

Corresponding author: Dr. Shailendra Segobin (segobin@cyceron.fr)

Full address: GIP Cyceron.
Boulevard Henri Becquerel
F-14074 Caen Cedex
France

Number of words in text: 4042

Number of tables: 1

Number of figures: 4

Number of supplementary materials: 0

Number of figures in supplementary materials: 0

Abstract

Background: The thalamus, a relay organ consisting of several nuclei, is shared between the frontocerebellar circuit and the Papez circuit, both particularly affected in Alcohol Use Disorder. Shrinkage of the thalamus is known to be more severe in alcoholics with Korsakoff's syndrome than in those without neurological complications (uncomplicated alcoholics). While thalamic atrophy could thus be a key factor explaining amnesia in Korsakoff's syndrome, the loci and nature of alterations within the thalamic nuclei in uncomplicated alcoholics and patients with Korsakoff's syndrome remains unclear. Indeed, the literature from animal and human models is disparate regarding whether the anterior thalamic nuclei, or the mediodorsal nuclei are particularly affected and would be responsible for amnesia

Methods: Sixty-two participants (20, healthy controls; 26 uncomplicated alcoholics and 16 patients with Korsakoff's syndrome) underwent a DTI sequence and T1-weighted MRI. State-of-the-art probabilistic tractography was used to segment the thalamus according to its connections to the prefrontal cortex and cerebellar Cruses I and II for the frontocerebellar circuit's executive loop, the precentral gyrus and cerebellar lobes IV-VI for the frontocerebellar circuit's motor loop, and hippocampus for the Papez circuit. The connectivity and volumes of these parcellations were calculated.

Results: Tractography showed that the hippocampus was principally connected to the anterior thalamic nuclei while the prefrontal cortex was principally connected to the mediodorsal nuclei. The fibre pathways connecting these brain regions and their respective thalamic nuclei have also been validated. ANCOVA, with age and gender as covariates, on connectivity measures showed abnormalities in both patient groups for thalamic parcellations connected to the hippocampus only ($F_{(2,57)}$=12·1; p<0·0001; η^2=0·2964; with graded effects of the number of connections from controls to UA to KS). Atrophy, on the other hand, was observed for the prefrontal parcellation in both patient groups and to the same extent compared to controls ($F_{(2,56)}$= 18·7; p<0·0001; η^2= 0·40). For the

hippocampus parcellation, atrophy was found in the KS group only ($F_{(2,56)}$= 5·5; p=0·006; η^2=0·170, corrected for multiple comparisons using Bonferroni, p<0.01). Post-hoc Tukey's test for unequal sample sizes, healthy controls > patients with Korsakoff's syndrome, p=0·0036).

Conclusions: Two different mechanisms seem to affect the thalamus. In the FCC, atrophy of the mediodorsal nuclei may lead the alterations, whereas in the PC, disconnection between the anterior nuclei and hippocampus may be the leading factor. Shrinkage of the anterior nuclei could be specific to KS patients, hence a potential neuroimaging marker of its pathophysiology, or more generally of thalamic amnesia for which KS has historically been used as a model.

Introduction

Korsakoff syndrome (KS) is a severe neurological disorder stemming from a combination of chronic and excessive alcohol consumption and altered thiamine metabolism (Kopelman *et al.*, 2009). It mainly results in severe amnesia and is potentially associated with executive deficits and ataxia. 'Uncomplicated' alcoholics (UA), i.e. patients with Alcohol Use Disorder (AUD) without such ostensible and severe neurological complications, are heterogeneous since some of them have preserved cognitive performances while others can have deficits close to those of KS patients (Pitel *et al.*, 2008).

In both UA and KS, two brain networks and associated cognitive functions are predominantly affected: the frontocerebellar circuit (FCC) and the Papez circuit (PC) (Chanraud *et al.*, 2010; Papez, 1937; Pitel *et al.*, 2014). Both functional circuits have been well described structurally in terms of gray matter (GM) nodes (Kelly and Strick, 2003; Papez, 1937) and the potential white matter tracts that connect them (Mori *et al.*, 2010; Segobin *et al.*, 2015). The FCC consists of two parallel closed loops, one executive (Brodmann areas 9 and 46; pons; cerebellar cruses I and II) and one motor (cerebellar lobes IV-VI; pons and motor cortex). The PC encompasses the hippocampus, mammillary bodies and cingulate gyrus. The thalamus is shared between the FCC and PC and has been described as "*the gateway to the cortex*" (Sherman and Guillery, 2001).

The effect of AUD on the thalamus has been documented mostly through the prism of KS via neuropathological and neuroimaging studies. In fact, KS patients have historically been used as a model for understanding the pathophysiological mechanisms underpinning thalamic/diencephalic amnesia (Kopelman, 2015). Generally, the thalamus was found to be affected in both UA and KS (Harding *et al.*, 2000; Kopelman *et al.*, 2009; Pitel *et al.*, 2014). Furthermore, graded effects were found in gray matter thalamic shrinkage from UA to KS patients (Pitel *et al.*, 2012; Sullivan and Pfefferbaum, 2008). Histological examinations have pointed towards the mediodorsal nuclei and the anterior nuclei of the thalamus as being especially affected in AUD (Harding *et al.*, 2000; Victor *et al.*,

1971). However, the specificity of these two nuclei, in terms of how they contribute towards the FCC or the PC, and how they are differentially altered in UA and KS patients, is still under debate (Aggleton, 2012; Carlesimo *et al.*, 2014; Kopelman, 2015; Pitel *et al.*, 2014). While several studies, involving both human and animal models, suggested that the mediodorsal nuclei could be critically affected in KS (Pitel *et al.*, 2012; Savage *et al.*, 2012; Victor *et al.*, 1971), hence explaining their anterograde amnesia, others have pointed towards lesions in the anterior nuclei as being key to this pathology (Harding *et al.*, 2000; Mair *et al.*, 1979; Mayes *et al.*, 1988).

Neuroimaging in humans has provided little to no evidence regarding the loci and nature of thalamic lesions at nuclear level. Conventional structural magnetic resonance imaging (MRI) sequences in the whole brain do not provide for high-resolution contrast between the different thalamic nuclei. However, development of diffusion tensor imaging (DTI) sequences, in tandem with state-of-the-art probabilistic tractography algorithms now allows the estimation of the number of white matter fibres connecting two regions at a voxel-level (Behrens *et al.*, 2007; Behrens, Johansen-Berg, *et al.*, 2003; Johansen-Berg *et al.*, 2005). It is therefore possible to segment the thalamus into parcellations that connect to key nodes of the FCC and PC, defined a priori, and estimate the number of fibre tracts contained in each parcellation. Corresponding volumes of these parcellations can subsequently be obtained through high-resolution T1-weighted MRI. Using these refined measurements, our objectives were 1) to identify which intra-thalamic regions the nodes of the FCC and PC were connected to, and 2) to specify the mechanisms (specific thalamic shrinkage and/or disconnection) that lead to the brain pathophysiology in UA and KS for each brain circuit.

Materials and Methods

Population

Forty-two patients (28 men, 14 women) with AUD (DSM-5 criteria, American Psychiatric Association, 2013) and 20 healthy subjects (15 men, 5 women) were included in the study.

Of those 42 AUD patients, 16 (7 men, 9 woman) filled the DSM–5 criteria for alcohol-induced major neurocognitive disorder, amnestic-confabulatory type, persistent and were therefore diagnosed as KS patients. They were recruited as inpatients at Caen University Hospital (n=8) and in a nursing home (Maison Vauban, Roubaix, France; n=8). All KS patients had a history of heavy drinking (longer than 20 years), but it was difficult to obtain accurate information about their alcohol intake due to their amnesia. The background information for the KS came mainly from family members and medical records. For each KS patient, the selection was made according to a codified procedure in a French officially registered centre for addiction. The case of each patient was examined by a multidisciplinary team made up of specialists in cognitive neuropsychology and behavioural neurology. A detailed neuropsychological examination enabled the diagnosis of all KS patients presenting disproportionately severe episodic memory disorders compared to other cognitive functions (Table 1). The consequences of their memory impairments were such that none of the KS were able to go back to their previous jobs and all of them lived in sheltered accommodation or were inpatients waiting for a place in an institution. Clinical and neuroimaging investigations ruled out other possible causes of memory impairments (particularly focal brain damage).

The 26 AUD patients without KS were considered as UA patients. They were recruited by clinicians while being inpatients for AUD at Caen University Hospital. Although patients were early in abstinence (16·7±21·4 days of sobriety prior to inclusion), none of them presented physical symptoms of alcohol withdrawal as assessed by the Cushman's scale (Cushman *et al.*, 1985) at inclusion. They were interviewed with the Alcohol Use Disorders Identification Test (AUDIT) (Gache *et al.*, 2005) and a modified version of the semi-structured lifetime drinking history (Pfefferbaum *et*

al., 1988). Measures included the duration of alcohol use (in years), alcohol misuse (in years), number of withdrawal and daily alcohol consumption prior to treatment (in units, a standard drink corresponding to a beverage containing 10g of pure ethanol).

The control group (healthy controls, HC) was recruited locally and to match the demographics of the UA patients. Inclusion criteria were: a minimum MMSE score of 26 or a minimum MATTIS score of 129, and a maximum Beck Depression Inventory (BDI) of 29. The maximum AUDIT score was 6 for women and 7 for men.

To be included, all participants had to be between 18 and 70 years old, and to have French as their native language. No participant had a comorbid psychiatric disorder, was under psychotropic medication, had a history of serious chronic pathology (diabetes, hepatitis, HIV, endocrinal disorder, as revealed by participants' blood tests), neurological problems (traumatic head injury causing loss of consciousness for >30 minutes, epilepsy, stroke, etc.) that might have affected cognitive function. No participant fulfilled the DSM-5 criteria for use disorder to another substance over the last 3 months (except tobacco). They had not taken any other psychoactive substance for more than 5 times over the last month (except alcohol for the patients). All participants were also evaluated for any signs of lacunar stroke, small vessel diseases or any overt vascular damage. We systematically performed this evaluation through a FLAIR sequence and a T2* sequence. The images were scrutinised by a neurologist who validated the inclusion of the patient in our research protocol, having excluded patients that potentially showed any form of neurological alterations due to any pathology other than linked with the pathophysiology of alcohol use disorder. All participants gave their informed written consent to the study, which was approved by the local ethics committee. The study was carried out in line with the Declaration of Helsinki (1964).

UA and HC were age- and education-matched (p=0·72 and p=0·76 respectively). KS differed from both HC and UA in age, education (years of schooling) and MMSE scores. Age, education, depression

(BDI), and anxiety scores (State-Trait Anxiety Inventory (STAI) (Spielberger CD, Gorsuch RL, Lushene R, Vagg PR, 1983) as well as nicotine dependence level are reported in Table 1.

Acquisition of neuroimaging data

Volumetric data

A high-resolution T1-weighted anatomical image was acquired for each subject on a Philips Achieva 3T (Netherlands) scanner using a three-dimensional fast-field echo sequence (sagittal; repetition time, 20 ms; echo time, 4.6ms; flip angle, 10°; 180 slices; slice thickness, 1 mm; field of view, 256x256 mm^2; matrix, 256x256).

DTI data

All participants also underwent a DTI sequence on the same scanner. 70 slices (slice thickness of 2mm, no gap) were acquired axially using a diffusion weighted imaging spin echo (DWI-SE) sequence (32 directions at b=1000 s/mm^2, repetition time=10000 ms; echo time=82 ms; flip angle=90°, field of view=224x224 mm^2; matrix=112x112 and in-plane resolution of 2x2 mm^2). One no-diffusion weighted image at b=0 s/mm^2 was also acquired.

Processing of neuroimaging data

Volumetric data processing

Volumetric datasets were pre-processed using the SPM12 toolbox (https://www.fil.ion.ucl.ac.uk/spm/software/spm12/ Statistical Parametric Mapping software; Wellcome Department of Cognitive Neurology, Institute of Neurology, London, UK). T1-weighted images were segmented into gray matter (GM) and spatially normalised to the Montreal Neurological Institute (MNI) space (voxel size=1.5 mm^3; matrix=121 x 145 x 121). The normalised GM images were modulated by the Jacobian determinants to preserve volume concentrations. The normalisation parameters (forward and inverse) were also saved to generate the required thalamic

seed and regional target masks for the thalamus classification step, and for the subsequent calculation of thalamic parcellated volumes. The flowchart describing the image processing steps is shown in Figure 1.

DTI data processing

The DWI-SE images for all subjects were pre-processed using the FSL 5.0.9 Diffusion Toolbox(Smith *et al.*, 2004) (FDT) (http://fsl.fmrib.ox.ac.uk/fsl/fslwiki/FDT). For each subject, the DWI images were first corrected for distortions due to Eddy currents and aligned to the b=0 s/mm^2 image using rigid-body registration for motion correction. Then, diffusion parameters at each voxel in the whole brain were first estimated using latest version of BEDPOST (Behrens, Woolrich, *et al.*, 2003). The resulting distributions were then used for connectivity-based classification of the thalamus using latest version of PROBTRACK (Behrens *et al.*, 2007). The algorithm basically evaluates connectivity values between the seed (thalamus) and the target masks defined a priori. The target masks used in the present study were (1) '*frontal-executive*' which included BA9 and BA46; (2) '*cerebellar-executive*' consisting of cerebellar crus I and II; (3) '*frontal-motor*' containing the precentral gyrus; (4) '*cerebellar-motor':* cerebellar lobs IV – VI, as key nodes of the FCC; and (5) *hippocampus* as a key node for the PC. The classification was carried out in native DTI image space. The output from PROBTRACK was a seed image for each target (5 images per subject on the overall) in which each voxel held the number of samples from that voxel to the relevant target mask. The value of all voxels outside the seed mask was zero. The number of samples in a thalamic voxel effectively refers to the number of streamlines in that voxel that will reach the target region. It represents a quantitative indication of the likelihood of a path existing between the seed and target region. The higher the number, the higher the likelihood that seed and target region are well-connected, thus providing an indication of the global connectivity existing between them.

Extracting number of samples and volumes

Using the five seed images, the thalamus was then individually segmented by classifying each of its voxels as belonging to the target mask with the highest number of samples, reflecting the highest connection probability (Behrens *et al.*, 2007; Behrens, Johansen-Berg, *et al.*, 2003). Thalamic voxels could be wrongly segmented as reflected by a low number of samples for each target mask in the seed images (Figure 2). A low number of samples can be recorded in a voxel for two main reasons. First, it can be related to the fact that the voxel is effectively connected to a region that has not been defined as an a priori target mask. The number recorded is thus noise in the data and should be ignored. Second, the pathology can result in a disconnection between the thalamus and a specific brain region such that the number of samples decreases drastically. Despite its low value, this voxel should not be ignored in the subsequent calculation of the mean number of samples connected to the target mask. Prior to performing a hard-segmentation of the thalamus, the seed images had to be thresholded to eliminate noise while keeping the voxels in which low values could be explained by the inherent pathology. To date, there is no standard methodology regarding thresholding of the number of samples resulting from probabilistic tractography to cater for noise (Morris *et al.*, 2008). Previous studies have intuitively chosen to threshold data at n=2 from 5000 (Fan *et al.*, 2016), n=10 from 5000 (Heiervang *et al.*, 2006); n=25 out of 25000 samples (Johansen-Berg *et al.*, 2007). The use of histograms has allowed for a data-driven way of selecting a threshold value. Histograms are very useful as it they allows for a visual representation of data distributions, hence facilitating the localisation of noise within the data, observed as a high frequency of low numbers on the plot (reference, figure 2, bottom part). For the control group, the noise distribution becomes less as the histograms start to "plateau". However, for the patients' groups, the "curve" before the plateau could be important, as these values could be a mixture of noise and a low number of samples due to the inherent pathology (figure 2, top part, line profile highlighting what could be such low values). In the absence of a gold standard as to how to threshold such measurements, we drew a horizontal line where the histograms generally start to curve, measured the corresponding x-values (number of samples) and calculated an average of those measurements. This cut-off number was found to be

equal to 35. Nevertheless, this threshold value remains an approximation that would very likely vary due to sample size, or different patient groups.

Post-segmentation, the mean number of samples in each parcellation was calculated for each subject in their native space. To calculate the volumes of these parcellations, the segmented thalami for each subject were warped to their corresponding GM volumes in MNI space by applying the forward transformation parameters from the normalisation process and the sum of the number of modulated GM voxels calculated from there.

The digital thalamic atlas (Krauth *et al.*, 2010), derived from histological data, was used to identify the parcellations that the target regions were connected to. This was conducted in controls first (to visually assess for consistency) and then in each and every patient.

Statistical analyses

For each thalamic parcellation, one-way analysis of covariance (ANCOVA) was performed to analyse group effect (HC, UA, and KS) for connectivity measures (mean number of samples) and volumes with age, gender and total intercranial volume as covariates. The main effects were corrected for multiple comparisons using a Bonferroni correction accounting for the 5 thalamic parcellations (new significant p-value < 0.01). The effect sizes for DTI and volumetric measures were also calculated (η^2). Post-hoc (HSD Tukey, unequal sample sizes) comparisons between HC, UA and KS groups were then performed. Over and above the debates on how multiplicity should be corrected for (Schulz and Grimes, 2005), we also considered the fact that the ANCOVAs already consider the 3 groups and that volumetric measures are not independent of the connectivity measures. These tests, and the number of comparisons therefore offer a good compromise and maintain the confidence and integrity of our statistical analyses. Correlations between connectivity and volumetric measurements on one hand, and alcohol drinking history on the other hand, with age and gender as covariates, were also carried out.

Data Availability

All data and materials used within this study will be made available, upon reasonable request, to research groups wishing to reproduce/confirm our results.

Results

Segmentation results were visually labelled using the thalamic histological atlas (Figure 3) and revealed that the 'frontal-executive' target had a high number of connections to a major portion of the mediodorsal nuclei and a small part of the ventral anterior nuclei (Krauth *et al.*, 2010). The 'cerebellar-executive' target had a high number of connections essentially to the ventral anterior nuclei and a small part of the mediodorsal nuclei. The 'frontal-motor' target was mainly connected to the ventral lateral and latero-dorsal part of the thalamus, while the 'cerebellar-motor' was mostly connected to the ventral lateral part of the thalamus and part of the lateral geniculate. The hippocampus had a high number of connections to the anterior nuclei and the ventral midline nuclei (part of the mediodorsal nuclei in atlas), pulvinar and latero-dorsal nuclei. For ease of comprehension, the parcellations connected to their respective targets will henceforth be referred to as *'frontal-executive parcellation'*, *'cerebellar-executive parcellation'*, *'frontal-motor parcellation'*, *'cerebellar-motor parcellation'* and *'hippocampus-parcellation'* respectively.

The ANCOVAs conducted on the connectivity measures showed significant between-group differences for the 'hippocampus-parcellation' only ($F_{(2,57)}$=12·1; p<0·0001; η^2=0·2964). Post-hoc comparisons revealed graded effects from HC to UA (p=0·002) to KS (p=0·0001) and UA to KS (p=0·0169).

Regarding the volumes of the thalamic parcellations, significant differences were observed for the *'frontal-executive parcellation'* ($F_{(2,56)}$=18·7; p<0·0001; η^2=0·40), and 'hippocampus parcellation' ($F_{(2,56)}$= 5·5; p=0·0060; η^2=0·170). Subsequent post-hoc comparisons showed lower volumes in the

'frontal-executive parcellation' in UA (p<0·0001) and KS compared to HC (p<0·0001). The *'hippocampus parcellation'* had significantly lower volumes only in the KS group compared to HC (p= 0·0036). The total volume of the thalamus also differed significantly ($F_{(2,56)}$= 12·6; p<0·0001; η^2= 0·310) between the 3 groups, with graded effects from HC and UA (p<0·0001), HC and KS (p<0·0001) and UA and KS (p=0·0275)both the UA and KS groups being significantly different from HC in post-hoc comparisons (p<0·0001). For all other parcellations and the whole thalamus, volumetric differences between UA and KS groups were not significant (Figure 4).

There were no significant correlations between alcohol drinking history and DTI, nor volumetric measurements (all p values > 0·05).

Discussion

Our results show that connections to the nodes of the FCC and PC are not limited to one nucleus only within the thalamus. The scientific explanation would be that thalamic nuclei are interconnected and the tractography algorithm independently evaluates the number of samples within each parcellation for every voxel. From a methodological point of view, the overlap between one or more nuclei for each parcel could be a resolution consideration. Nevertheless, the scientific explanation is more potent since it has been shown that the effective resolution of the resulting parcellations should be finer than that of the original diffusion images as the tractography algorithm works on diffusion measurements on a global scale rather than at a voxel level (Johansen-Berg et al., 2005).

The present study showed that the motor loop of the FCC is mostly connected to the ventral lateral and lateral-dorsal part of the thalamus, which is consistent with previous studies showing the functional-anatomical involvement of the thalamus within this loop in healthy subjects, (Johansen-Berg *et al.*, 2005) and in patients with tremors (Fang *et al.*, 2016). The absence of between-group difference for the 'frontal-motor parcellations' probably implies that this part of the FCC circuitry is relatively preserved in AUD as has been previously reported (Harper, 2009). On the executive front, the connections between the cerebellum and specific thalamic nuclei have not been well

documented in the literature. In fact, the perspective of the cerebellum playing a role in cognition, above motor performances, is fairly new (Buckner, 2013), which in-part explains why no studies in humans have specifically pointed to thalamic nuclei that connect to the cerebellar cruses. The present investigation and previous studies (Behrens, Johansen-Berg, *et al.*, 2003; Johansen-Berg *et al.*, 2005) suggest that the nuclei connected to the cerebellar-executive regions (ventral anterior and mediodorsal nuclei) are also connected to the frontal part of the executive loop.

That the hippocampus has connections to several thalamic nuclei fits well with the literature on hippocampo-thalamo connectivity. While connections between the anterior nuclei and hippocampus via the fornix is well established, non-fornical projections via the entorhinal cortex to the medial nuclei, pulvinar and part of the lateral-dorsal nuclei have also been observed using tracer techniques in macaques (Saunders *et al.*, 2005). In healthy humans, probabilistic tractography between the medial temporal lobe and the thalamus has confirmed these non-fornical fibre projections (Johansen-Berg *et al.*, 2005). Several animal and human studies (Aggleton and Brown, 1999; Carlesimo *et al.*, 2011, 2014; Mitchell and Chakraborty, 2013), some involving resting-state fMRI (Kafkas and Montaldi, 2014), have highlighted the implication of the mediodorsal nuclei in memory functioning through this non-fornical route. In fact, the implication of which specific nuclei, anterior or mediodorsal, whose lesions contribute directly towards amnesia, has so far been elusive (Mair *et al.*, 2015).

In order to understand why part of the mediodorsal nuclei, known to be rather involved in higher order cognitive functions than in episodic memory, could contribute to amnesia, calculations were made a-posteriori using a histological atlas (Krauth *et al.*, 2010). These showed that 83·9% of the anterior nuclei were involved in the hippocampus-parcellations (13·9% of the mediodorsal nuclei, 29·2% of pulvinar, and 14·1% of lateral-dorsal). The atlas is known to have limitations regarding accurate quantitation (Pergola, 2016) and does not contain the smaller nuclei like the reuniens and rhomboid nuclei, both suspected to be involved in diencephalic amnesia (Barnett *et al.*, 2018). A

further detailed visual inspection of the atlas has allowed us to observe that these nuclei are potentially included in the mediodorsal nuclei indices of the atlas, hence offering an alternative explanation to the observed direct connections between the so-called mediodorsal nuclei and the hippocampus and its subsequent implication in memory. Taken together, it can be assumed that it is the anterior nuclei that are mainly and directly connected to the hippocampus. Similar calculations were done for the frontal-executive parcellations and it was found that 70·1% of the mediodorsal nuclei were involved in that parcellation. Hence, it can be assumed that the mediodorsal nuclei are mainly connected to the frontal-executive target.

These neuroanatomical findings are crucial to the better understanding of the pathophysiology of AUD as they allow the specification of the nature of the structural damage occurring within thalamic nuclei (Harding *et al.*, 2000; Mair *et al.*, 1979; Mayes *et al.*, 1988). The novelty of the present study is to involve UA and KS patients having brain abnormalities along a continuum that is known to slowly evolve from mild-to-moderate-to-severe so that we can concretely formulate a general model of specific thalamic structural alterations happening in the pathology. In AUD, two distinct pathophysiological mechanisms may thus affect the PC and FCC. In the PC, disconnection between the hippocampus and its related thalamic parcellation, involving mainly the anterior nuclei, may be leading the alterations. In the FCC, shrinkage of the 'frontal-executive' parcellation, involving mainly the mediodorsal nuclei, seems to be the most prominent. These results are in agreement with previously reported findings in animal, histological and neuroimaging studies that both the anterior and mediodorsal thalamus are severely damaged in KS (Harding *et al.*, 2000; Mair *et al.*, 1979; Mayes *et al.*, 1988; Savage *et al.*, 2012). While the extent of damage to the mediodorsal nuclei is similar in UA and KS, shrinkage of the anterior nuclei seems specific to KS. Having showed that the mechanism that leads the pathophysiology of alterations in the anterior nuclei of the thalamus in AUD is a disconnection, it can be hypothesized that this graded disconnection among AUD groups potentially cascades into atrophy of the anterior thalamus, leading to KS. This would corroborate with case studies in KS that have found disruption of the mammillothalamic tract and lesions within the

anterior nuclei and mammillary bodies (Mair *et al.*, 1979; Mayes *et al.*, 1988). A quantitative histological study has also echoed the same findings (Harding *et al.*, 2000), pinpointing to the anterior nuclei as being a critical site of damage in patients with KS. Nevertheless, a couple of studies have found the mediodorsal nuclei to be significantly atrophied in KS patients compared to controls (Victor *et al.*, 1971), and KS patients compared to both UA and controls (Pitel *et al.*, 2012). Over and above the criticism regarding the neuropsychological criteria that were used to fit the aetiology of KS patients in the study by Victor and colleagues, another potential explanation is that what is identified as being part of the mediodorsal nuclei is in fact a thalamic region that effectively houses the reuniens and rhomboid nuclei involved in memory functions (Barnett *et al.*, 2018). This is also reflected in one neuroimaging study (Pitel *et al.*, 2012) in which, from the results portrayed, atrophy of the thalamus is evident on both the anterior as well as part of the mediodorsal front.

It was surprising to find no significant between-group difference for the 'cerebellar-executive parcellations', which is known to be altered in AUD. The reason could be methodological as the brainstem, midbrain and cerebellum contain dense crossing fibres that make tracking of pathways difficult. Yet, this did not seem to be the case for the 'cerebellar-motor' target in which the fibre tracts go through these same regions. Another reason could be that the leading mechanism is a demyelination, as reflected through decrease in FA values in the inferior and superior cerebellar peduncles, but is not necessarily accompanied by neuronal death, such that the number of connections does not necessarily decrease. The absence of between-group difference for the 'frontal-motor parcellations' probably implies that this part of the FCC circuitry is relatively preserved in AUD as has been previously reported.

For the cerebellar-motor parcellation, the presence of an outlier could be a reason for why no significant comparisons were observed ($F(2,55) = 3.8782$; $p=0.0266$ if outlier is not considered in the stats). However, interpretation of results from this parcellation was not deemed comparable to the hippocampus parcellation since no significant results were obtained on the connectivity side.

Atrophy of the cerebellar-motor parcellation could therefore be a consequence within the main pathophysiological mechanism of KS.

Methodological and statistical considerations

Cortical atrophy has not been explicitly accounted for. However, it has been indirectly considered as tractography is performed in native space. The seed and target masks have been obtained from MNI space, segmented and normalized into native space and should technically not contain atrophied voxels. However, it is difficult to say whether cortical atrophy needs to be corrected for or not, as structural disconnection could induce atrophy and vice-versa. While the relationships between thalamic atrophy and disconnections are complex to interpret at the current stage, what is interesting is that we observe clearly defined mechanisms across 2 groups of patients that lie along a continuum, such that we can suppose which mechanisms are more prominent in their respective brain circuits as detailed above.

Conclusion

Overall, the results of this study show, in-vivo and across a continuum of AUD pathology, that the chronic and excessive consumption of alcohol is associated with structural damage to both the mediodorsal and anterior nuclei. However, despite a relatively small but robust sample size, atrophy of the anterior nuclei has shown a tendency to be specific to KS patients and offers the prospect of being a neuroimaging marker that could define not only the pathophysiology of KS but also that of other neurological disorders directly linked to thalamic amnesia. Further studies should be geared towards confirming this line of thought.

Acknowledgements

This study was funded by Fondation pour la Recherche Medicale (FRM, ING20140129160), ANR-Retour post-doctorant 2010, Conseil Regional Basse Normandie, and MILDECA.

Conflicts of Interest

All authors declare no conflict of interest in any form or kind in relation to this study and its publication.

References

Aggleton JP. Multiple anatomical systems embedded within the primate medial temporal lobe: Implications for hippocampal function [Internet]. Neurosci. Biobehav. Rev. 2012; 36: 1579–1596.Available from: http://www.sciencedirect.com/science/article/pii/S0149763411001722

Aggleton JP, Brown MW. Episodic memory, amnesia, and the hippocampal-anterior thalamic axis. [Internet]. Behav. Brain Sci. 1999; 22: 425-44; discussion 444-89.Available from: http://www.ncbi.nlm.nih.gov/pubmed/11301518

Barnett SC, Perry BAL, Dalrymple-Alford JC, Parr-Brownlie LC. Optogenetic stimulation: Understanding memory and treating deficits [Internet]. Hippocampus 2018; 28: 457–470.Available from: https://onlinelibrary.wiley.com/doi/abs/10.1002/hipo.22960

Behrens TEJ, Berg HJ, Jbabdi S, Rushworth MFS, Woolrich MW. Probabilistic diffusion tractography with multiple fibre orientations: What can we gain? [Internet]. Neuroimage 2007; 34: 144–55.[cited 2013 Mar 1] Available from: http://www.ncbi.nlm.nih.gov/pubmed/17070705

Behrens TEJ, Johansen-Berg H, Woolrich MW, Smith SM, Wheeler-Kingshott CAM, Boulby PA, et al. Non-invasive mapping of connections between human thalamus and cortex using diffusion imaging [Internet]. Nat Neurosci 2003; 6: 750–757.Available from: http://dx.doi.org/10.1038/nn1075

Behrens TEJ, Woolrich MW, Jenkinson M, Johansen-Berg H, Nunes RG, Clare S, et al. Characterization and propagation of uncertainty in diffusion-weighted MR imaging. [Internet]. Magn. Reson. Med. 2003; 50: 1077–88.[cited 2013 Feb 28] Available from: http://www.ncbi.nlm.nih.gov/pubmed/14587019

Buckner RL. The cerebellum and cognitive function: 25 years of insight from anatomy and neuroimaging [Internet]. Neuron 2013; 80: 807–815.Available from: http://dx.doi.org/10.1016/j.neuron.2013.10.044

Carlesimo GA, Lombardi MG, Caltagirone C. Vascular thalamic amnesia: A reappraisal [Internet]. Neuropsychologia 2011; 49: 777–789.Available from: http://www.sciencedirect.com/science/article/pii/S0028393211000315

Carlesimo GA, Lombardi MG, Caltagirone C, Barban F. Recollection and familiarity in the human thalamus [Internet]. Neurosci. Biobehav. Rev. 2014; 54: 18–28.Available from: http://dx.doi.org/10.1016/j.neubiorev.2014.09.006

Chanraud S, Pitel A-L, Rohlfing T, Pfefferbaum A, Sullivan E V. Dual tasking and working memory in alcoholism: relation to frontocerebellar circuitry. [Internet]. Neuropsychopharmacology 2010; 35: 1868–78.[cited 2012 Jul 19] Available from: http://www.pubmedcentral.nih.gov/articlerender.fcgi?artid=2919220&tool=pmcentrez&rendertype=abstract

Cushman PJ, Forbes R, Lerner W, Stewart M. Alcohol withdrawal syndromes: clinical management with lofexidine. Alcohol Clin Exp Res. 1985; 9: 103–108.

Fan L, Li H, Zhuo J, Zhang Y, Wang J, Chen L, et al. The Human Brainnetome Atlas: A New Brain Atlas Based on Connectional Architecture. Cereb. Cortex 2016; 26: 3508–3526.

Fang W, Chen H, Wang H, Zhang H, Puneet M, Liu M, et al. Essential tremor is associated with disruption of functional connectivity in the ventral intermediate Nucleus-Motor Cortex-Cerebellum circuit. Hum. Brain Mapp. 2016; 37: 165–178.

Gache P, Michaud P, Landry U, Accietto C, Arfaoui S, Wenger O, et al. The Alcohol Use Disorders Identification Test (AUDIT) as a Screening Tool for Excessive Drinking in Primary Care: Reliability and Validity of a French Version. Alcohol Clin Exp Res. 2005; 29: 2001–2007.

Harding A, Halliday G, Caine D, Kril J. Degeneration of anterior thalamic nuclei differentiates

alcoholics with amnesia. [Internet]. Brain 2000; 123 (Pt 1: 141–54.Available from: http://www.ncbi.nlm.nih.gov/pubmed/10611128

Harper C. The neuropathology of alcohol-related brain damage. [Internet]. Alcohol Alcohol 2009; 44: 136–40.[cited 2014 Jul 10] Available from: http://www.ncbi.nlm.nih.gov/pubmed/19147798

Heiervang E, Behrens TEJ, Mackay CE, Robson MD, Johansen-Berg H. Between session reproducibility and between subject variability of diffusion MR and tractography measures [Internet]. Neuroimage 2006; 33: 867–877.Available from: http://www.sciencedirect.com/science/article/pii/S1053811906008081

Johansen-Berg H, Behrens TEJ, Sillery E, Ciccarelli O, Thompson AJ, Smith SM, et al. Functional-anatomical validation and individual variation of diffusion tractography-based segmentation of the human thalamus. Cereb. Cortex 2005; 15: 31–39.

Johansen-Berg H, Della-Maggiore V, Behrens TEJ, Smith SM, Paus T. Integrity of white matter in the corpus callosum correlates with bimanual co-ordination skills. Neuroimage 2007; 36 Suppl 2: T16-21.

Kafkas A, Montaldi D. Two separate, but interacting, neural systems for familiarity and novelty detection: A dual-route mechanism [Internet]. Hippocampus 2014; 24: 516–527.Available from: http://dx.doi.org/10.1002/hipo.22241

Kelly RM, Strick PL. Cerebellar loops with motor cortex and prefrontal cortex of a nonhuman primate. [Internet]. J. Neurosci. 2003; 23: 8432–44.Available from: http://www.ncbi.nlm.nih.gov/pubmed/12968006

Kopelman MD. What does a comparison of the alcoholic Korsakoff syndrome and thalamic infarction tell us about thalamic amnesia? [Internet]. Neurosci. Biobehav. Rev. 2015; 54: 46–56.Available from: http://www.sciencedirect.com/science/article/pii/S0149763414002127

Kopelman MD, Thomson AD, Guerrini I, Marshall EJ. The Korsakoff syndrome: clinical aspects, psychology and treatment. [Internet]. Alcohol Alcohol 2009; 44: 148–54.[cited 2013 Aug 15] Available from: http://www.ncbi.nlm.nih.gov/pubmed/19151162

Krauth A, Blanc R, Poveda A, Jeanmonod D, Morel A, Székely G. A mean three-dimensional atlas of the human thalamus: generation from multiple histological data. [Internet]. Neuroimage 2010; 49: 2053–62.[cited 2013 Oct 30] Available from: http://www.ncbi.nlm.nih.gov/pubmed/19853042

Mair RG, Miller RLA, Wormwood BA, Francoeur MJ, Onos KD, Gibson. BM. The neurobiology of thalamic amnesia: Contributions of medial thalamus and prefrontal cortex to delayed conditional discrimination [Internet]. Neurosci. Biobehav. Rev. 2015; 54: 161–174.Available from: http://www.sciencedirect.com/science/article/pii/S0149763415000135

Mair WGP, Warrington EK, Weiskrantz L. Memory disorder in Korsakoff's psychosis: a neuropathological and neuropsychological investigation of two cases. [Internet]. Brain 1979; 102: 749–783.Available from: http://brain.oxfordjournals.org/content/102/4/749.abstract

Mayes AR, Meudell PR, Mann D, Pickering A. Location of Lesions in Korsakoff's Syndrome: Neuropsychological and Neuropathological Data on Two Patients [Internet]. Cortex 1988; 24: 367–388.Available from: http://www.sciencedirect.com/science/article/pii/S0010945288800017

Mitchell AS, Chakraborty S. What does the mediodorsal thalamus do? [Internet]. Front. Syst. Neurosci. 2013; 7: 37.Available from: http://www.pubmedcentral.nih.gov/articlerender.fcgi?artid=3738868&tool=pmcentrez&rendertype=abstract

Mori S, van Zijl PCM, Oishi K, Faria A V. MRI Atlas of Human White Matter 2nd Edition [Internet]. Elsevier Science; 2010. Available from: http://books.google.fr/books?id=v8MWjTpVUAYC

Morris DM, Embleton K V, Parker GJM. Probabilistic fibre tracking: Differentiation of connections from chance events [Internet]. Neuroimage 2008; 42: 1329–1339.Available from:

http://www.sciencedirect.com/science/article/pii/S1053811908007301

Papez J. A proposed mechanism of emotion. Arch Neurol Psychiatry 1937; 28: 725–743.

Pergola G. Thalamic amnesia after infarct: The role of the mammillothalamic tract and mediodorsal nucleus. Neurology 2016; 86: 1928.

Pfefferbaum A, Rosenbloom M, Crusan K, Jernigan TL. Brain CT Changes in Alcoholics: Effects of Age and Alcohol Consumption [Internet]. Alcohol. Clin. Exp. Res. 1988; 12: 81–87.Available from: http://dx.doi.org/10.1111/j.1530-0277.1988.tb00137.x

Pitel AL, Beaunieux H, Witkowski T, Vabret F, de la Sayette V, Viader F, et al. Episodic and working memory deficits in alcoholic Korsakoff patients: the continuity theory revisited. [Internet]. Alcohol. Clin. Exp. Res. 2008; 32: 1229–41.[cited 2013 Mar 6] Available from: http://www.ncbi.nlm.nih.gov/pubmed/18482159

Pitel AL, Chételat G, Le Berre a P, Desgranges B, Eustache F, Beaunieux H. Macrostructural abnormalities in Korsakoff syndrome compared with uncomplicated alcoholism. [Internet]. Neurology 2012; 78: 1330–3.Available from: http://www.ncbi.nlm.nih.gov/pubmed/22496200

Pitel AL, Segobin SH, Ritz L, Eustache F, Beaunieux H. Thalamic abnormalities are a cardinal feature of alcohol-related brain dysfunction [Internet]. Neurosci. Biobehav. Rev. 2014; 54: 38–45.Available from: http://dx.doi.org/10.1016/j.neubiorev.2014.07.023

Saunders RC, Mishkin M, Aggleton JP. Projections from the entorhinal cortex, perirhinal cortex, presubiculum, and parasubiculum to the medial thalamus in macaque monkeys: identifying different pathways using disconnection techniques. Exp. brain Res. 2005; 167: 1–16.

Savage LM, Hall JM, Resende LS. Translational rodent models of Korsakoff syndrome reveal the critical neuroanatomical substrates of memory dysfunction and recovery. Neuropsychol. Rev. 2012; 22: 195–209.

Schulz KF, Grimes DA. Multiplicity in randomised trials I: endpoints and treatments [Internet]. Lancet 2005; 365: 1591–1595.Available from: https://doi.org/10.1016/S0140-6736(05)66461-6

Segobin S, Ritz L, Lannuzel C, Boudehent C, Vabret F, Eustache F, et al. Integrity of white matter microstructure in alcoholics with and without Korsakoff's syndrome [Internet]. Hum. Brain Mapp. 2015; 36: 2795–2808.Available from: http://dx.doi.org/10.1002/hbm.22808

Sherman SM, Guillery RW. Chapter {III} - The Afferent Axons to the Thalamus [Internet]. In: Guillery SMSW, editor(s). Exploring the Thalamus. San Diego: Academic Press; 2001. p. 59–107.Available from: http://www.sciencedirect.com/science/article/pii/B9780123054609500174

Smith SM, Jenkinson M, Woolrich MW, Beckmann CF, Behrens TEJ, Johansen-Berg H, et al. Advances in functional and structural MR image analysis and implementation as FSL [Internet]. Neuroimage 2004; 23, Supple: S208–S219.Available from: http://www.sciencedirect.com/science/article/pii/S1053811904003933

Spielberger CD, Gorsuch RL, Lushene R, Vagg PR JG. Manual for the State-Trait Anxiety Inventory (form Y). Palo Alto: 1983.

Sullivan E V, Pfefferbaum A. Neuroimaging of the Wernicke-Korsakoff syndrome. [Internet]. Alcohol Alcohol 2008; 44: 155–65.[cited 2013 Aug 28] Available from: http://www.pubmedcentral.nih.gov/articlerender.fcgi?artid=2724861&tool=pmcentrez&rendertype=abstract

Victor M, Adams RD, Collins GH. The Wernicke- Korsakoff syndrome. Philadelphia: F.A. Davis Co.; 1971.

Legends

Figure 1: Processing steps for the anatomical T1-weighted image and the DTI sequence to output mean number of connections per sub-nuclei and their corresponding volumes. **STEP 1:** The T1W-MRI image is co-registered to the DWI image (b=0 image) and the forward transformation parameters mapping the transformation from T1W-MRI space (**M** matrix) and its inverse transformation parameters ($\mathbf{M}^{-1}$ matrix) are saved. **STEP 2:** The T1W-MRI image is also segmented in gray matter (accounting for brain size by multiplying with the Jacobian determinants) and spatially normalised to MNI space, and the warping parameters mapping the normalisation from native MRI to MNI space (**W** matrix) and its inverse ($\mathbf{W}^{-1}$ matrix) are also saved. **STEP 3:** The $\mathbf{W}^{-1}$ and **M** matrix transformations are successively applied to the target masks in MNI space to put them into DTI native space. **STEP 4:** The diffusion parameters are estimated using BEDPOST. **STEP 5:** the number of connections from each target mask to the seed mask (thalamus) is estimated using PROBTRACK which outputs one image for each target mask (RESULT (A), 5 images per subject on the overall). **STEP 6:** A hard-segmentation is performed on RESULT (A) to produce one image (RESULT (B)) where each voxel within the thalamus is assigned to the target mask that has the highest number of connections. Hence the nuclei are segmented. **STEP 7:** The segmented nuclei are used to calculate the mean number of connections from RESULT (A). **STEP 8:** The corresponding volumes of the nuclei are calculated by transforming RESULT (B) into MNI space using the $\mathbf{M}^{-1}$ and **W** transformation matrices and multiplying by the gray matter volume.

Figure 2: Top left brain image shows the seed results obtained for targets: hippocampus (red thalamic clusters) and frontal-executive (blue thalamic clusters). The contours of those two clusters are drawn on the top right brain image (red contour for hippocampus as a target and blue contour for the frontal-executive target). A profile has been drawn across the image (yellow line – corresponds to x-axis on top graph) and the voxel intensities (corresponds to y-axis on top graph) in the seed results are plotted on the graph at the top. These voxel intensities correspond to the number of DTI samples for each seed in their respective images. Histograms (bottom graph showing number of voxels in seed image containing the corresponding number of DTI samples) show how the cut-off of 35 was selected for thresholding for the frontal executive region. Low values that represent noise are likely to be in the 'vertical' part of the histogram. The range of values lying in the vertical area for all 3 groups were taken and averaged. This average number for the seeds converged towards n=35. Beyond n=35, the voxel values for each seed image for each subject started to plateau such that they can be considered to be part of the connectivity distribution and not noise. This cut-off (n=35) was consistent for all seed images and was therefore used across the whole dataset.

Figure 3: Thalamic parcellations that result from the segmentation using PROBTRACK, the thalamus used as a seed and the targets being the 'frontal-executive' (blue), 'frontal-motor' (red), 'cerebellar-executive' (green), 'cerebellar-motor'(yellow), and hippocampus (orange). First column shows the thalamic parcellations in the orthogonal views. Second column (far fight) shows the fibre tracts that effectively connect the thalamic parcellations to their respective targets, first in 2D-view, then in 3D-view. These tracts have been produced for graphical representation only. The figure has been rendered from the data of one healthy control in native space. This visual assessment also served as systematic quality control for all 62 participants.

Figure 4: Boxplots showing group comparisons (healthy controls (HC) v/s uncomplicated alcoholics (UA) v/s patients with Korsakoff's syndrome (KS)) for mean number of DTI samples and volumes for each thalamic parcellation.
+ denotes outliers within respective group, included in the statistical comparisons but excluded from boxplots when calculating median, lower and upper percentiles.
***** denotes subsequent significant differences between HC and UA and § denotes significant differences between UA and KS (post-hoc, Tukey, unequal sample sizes) $p<0.01$ (corrected for multiple comparisons for main effects and at post-hoc level, Tukey HSD for unequal sample sizes).

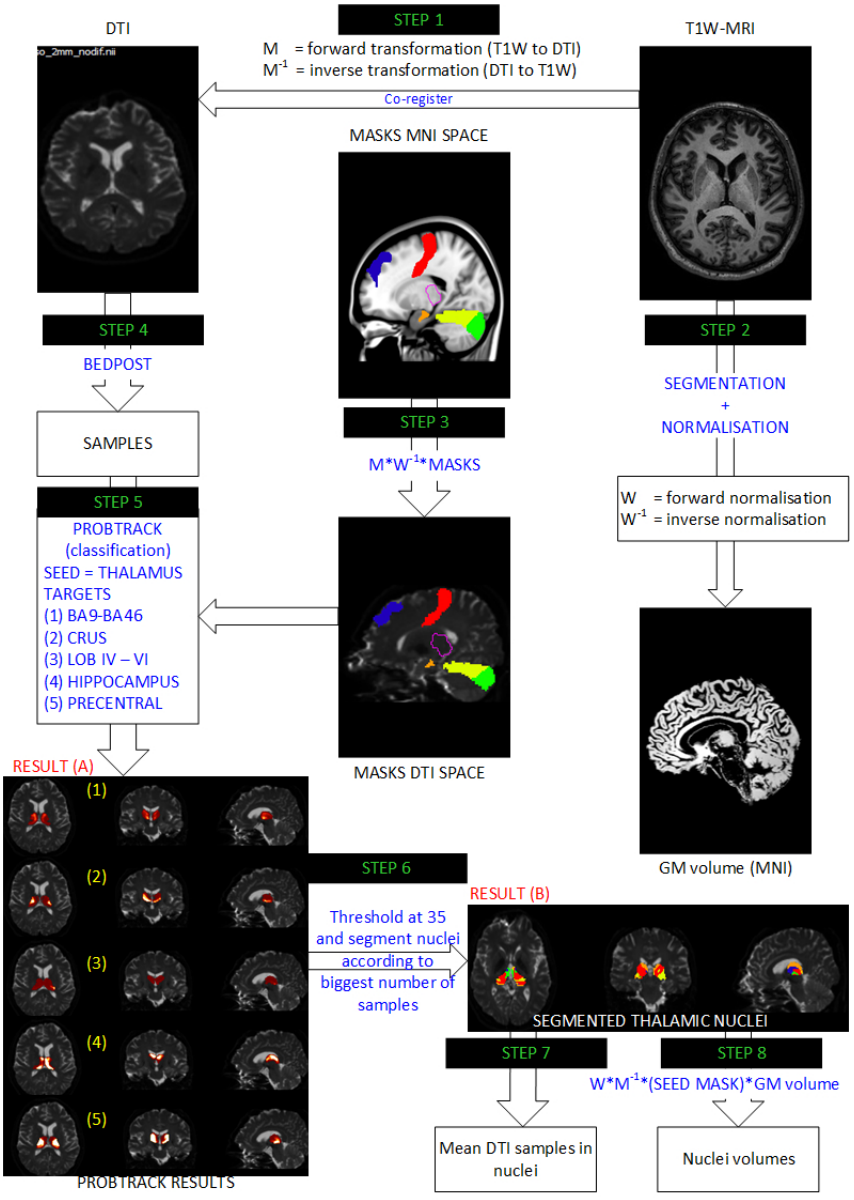

Figure 1: Processing steps for the anatomical T1-weighted image and the DTI sequence to output mean number of connections per sub-nuclei and their corresponding volumes. **STEP 1:** The T1W-MRI image is co-registered to the DWI image (b=0 image) and the forward transformation parameters mapping the transformation from T1W-MRI space (**M** matrix) and its inverse transformation parameters ($\mathbf{M^{-1}}$ matrix) are saved. **STEP 2:** The T1W-MRI image is also segmented in gray matter (accounting for brain size by multiplying with the Jacobian determinants) and spatially normalised to MNI space, and the warping parameters mapping the normalisation from native MRI to MNI space (**W** matrix) and its inverse ($\mathbf{W^{-1}}$ matrix) are also saved. **STEP 3:** The $\mathbf{W^{-1}}$ and **M** matrix transformations are successively applied to the target masks in MNI space to put them into DTI native space. **STEP 4:** The diffusion parameters are estimated using BEDPOST. **STEP 5:** the number of connections from each target mask to the seed mask (thalamus) is estimated using PROBTRACK which outputs one image for each target mask (RESULT (A), 5 images per subject on the overall). **STEP 6:** A hard-segmentation is performed on RESULT (A) to produce one image (RESULT (B)) where each voxel within the thalamus is assigned to the target mask that has the

highest number of connections. Hence the nuclei are segmented. **STEP 7:** The segmented nuclei are used to calculate the mean number of connections from RESULT (A). **STEP 8:** The corresponding volumes of the nuclei are calculated by transforming RESULT (B) into MNI space using the $\mathbf{M}^{-1}$ and **W** transformation matrices and multiplying by the gray matter volume.

210x297mm (96 x 96 DPI)

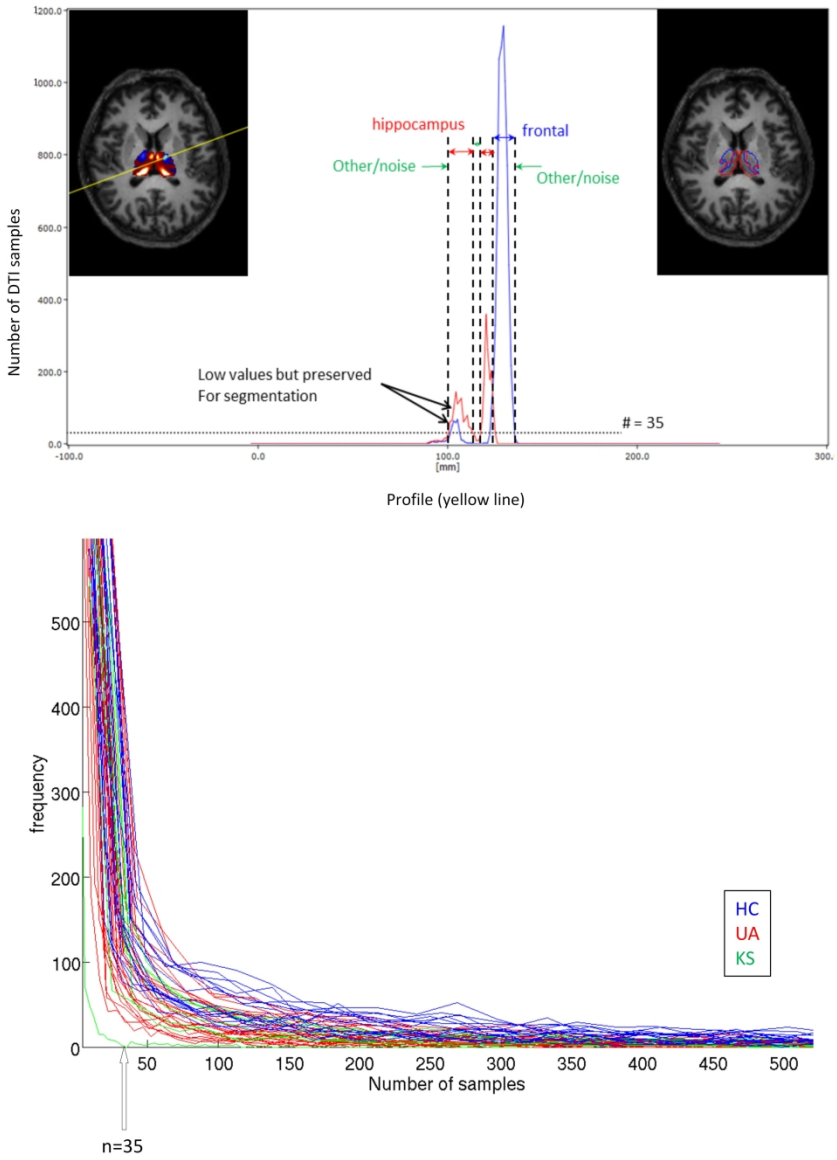

Figure 2: Top left brain image shows the seed results obtained for targets: hippocampus (red thalamic clusters) and frontal-executive (blue thalamic clusters). The contours of those two clusters are drawn on the top right brain image (red contour for hippocampus as a target and blue contour for the frontal-executive target). A profile has been drawn across the image (yellow line – corresponds to x-axis on top graph) and the voxel intensities (corresponds to y-axis on top graph) in the seed results are plotted on the graph at the top. These voxel intensities correspond to the number of DTI samples for each seed in their respective images. Histograms (bottom graph showing number of voxels in seed image containing the corresponding number of DTI samples) show how the cut-off of 35 was selected for thresholding for the frontal executive region. Low values that represent noise are likely to be in the 'vertical' part of the histogram. The range of values lying in the vertical area for all 3 groups were taken and averaged. This average number for the seeds converged towards n=35. Beyond n=35, the voxel values for each seed image for each subject started to plateau such that they can be considered to be part of the connectivity distribution and not noise. This cut-off (n=35) was consistent for all seed images and was therefore used across the whole dataset.

213x301mm (300 x 300 DPI)

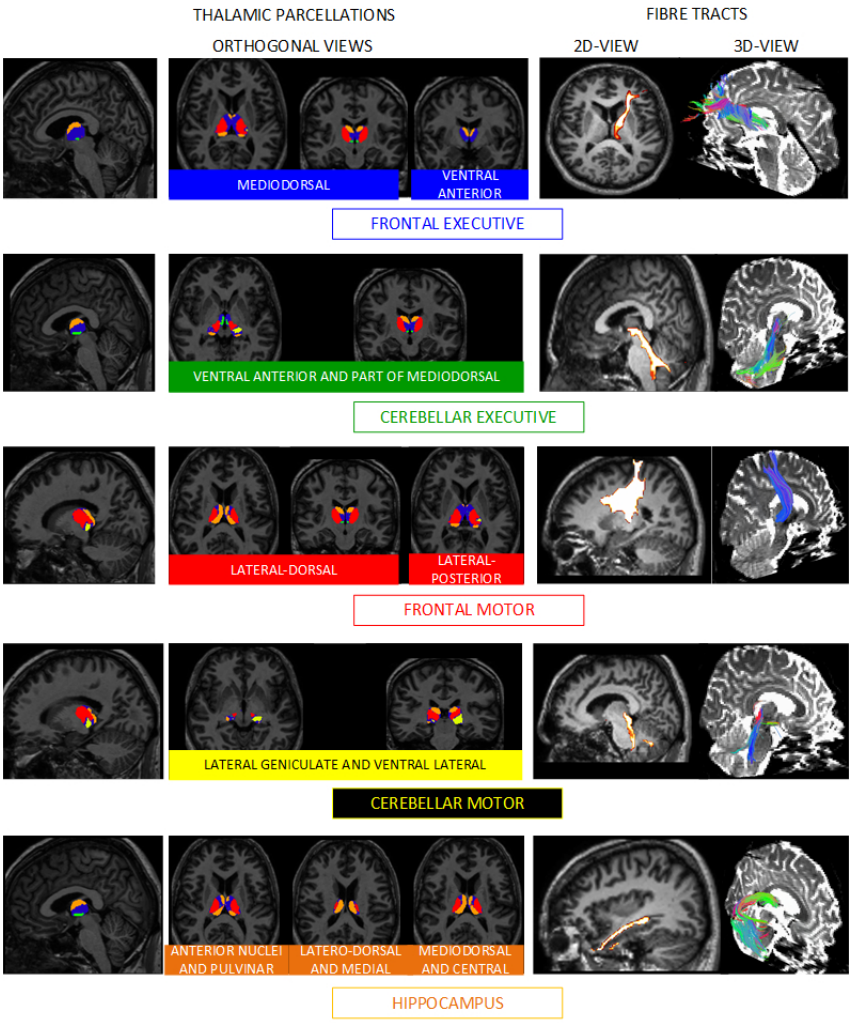

Figure 3: Thalamic parcellations that result from the segmentation using PROBTRACK, the thalamus used as a seed and the targets being the 'frontal-executive' (blue), 'frontal-motor' (red), 'cerebellar-executive' (green), 'cerebellar-motor'(yellow), and hippocampus (orange). First column shows the thalamic parcellations in the orthogonal views. Second column (far fight) shows the fibre tracts that effectively connect the thalamic parcellations to their respective targets, first in 2D-view, then in 3D-view. These tracts have been produced for graphical representation only. The figure has been rendered from the data of one healthy control in native space. This visual assessment also served as systematic quality control for all 62 participants.

210x297mm (96 x 96 DPI)

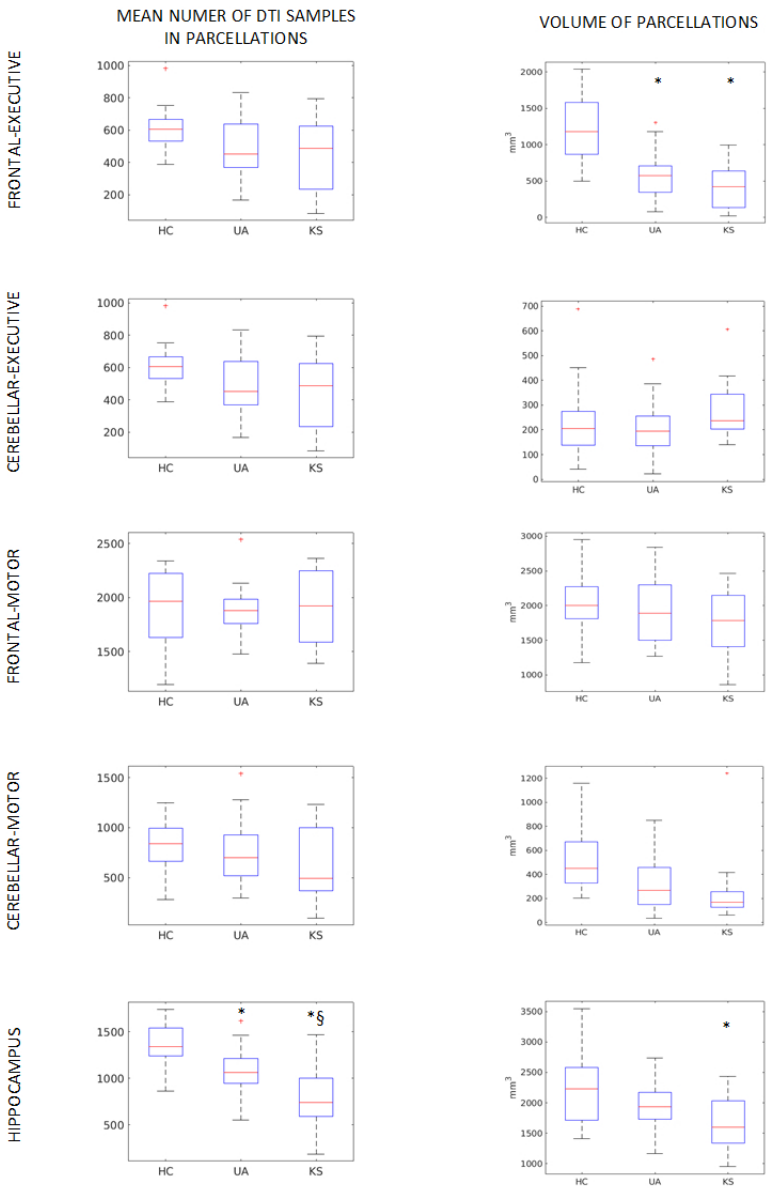

Figure 4: Boxplots showing group comparisons (healthy controls (HC) v/s uncomplicated alcoholics (UA) v/s patients with Korsakoff's syndrome (KS)) for mean number of DTI samples and volumes for each thalamic parcellation.+ denotes outliers within respective group, included in the statistical comparisons but excluded from boxplots when calculating median, lower and upper percentiles.* denotes subsequent significant differences between HC and UA and § denotes significant differences between UA and KS (post-hoc, Tukey, unequal sample sizes) $p<0.01$ (corrected for multiple comparisons for main effects and at post-hoc level, Tukey HSD for unequal sample sizes).

210x297mm (96 x 96 DPI)

Table 1: Demographic, clinical and neuropsychological description of the control participants and alcoholics with and without Korsakoff's syndrome.

Variable	HC (n=20) M=15;F=5	UA (n=26) M=21;F=5	KS (n=16) M=7;F=9	Group differences*
DEMOGRAPHIC DATA				
Age§ (years)	44·5±6·8 [31 - 55]	46·6±8·5 [33 - 66]	55·9±5·7 [44 - 67]	HC = UA; HC < KS (p=0·0002) UA < KS (p=0·0016)
Education (years)	11·5±2·1 [9-15]	11·9±1·9 [9-15]	9·9±2·1 [6-15]	HC = UA = KS
Alcohol Use Disorders Test (AUDIT)	2·8±1·5 [0 - 5]	29·4±6·9 [9 - 39]	15·0±13·6 [1 - 37]	HC < UA (p=0·0001) HC < KS (p=0·0034) KS < UA (p=0·0006)
Beck Depression Index (BDI)	3·8±3·7 [0 - 14]	11·3±7·4 [2 - 27]	7·9±8·0 [0 - 29]	HC < UA (p=0·0021) HC = KS UA = KS
STAI[a] A	27·3±7·0 [20 - 47]	29·9±10·4 [20 - 59]	30·5±9·5 [20 - 51]	HC = UA = KS
STAI[a] B	33·6±7·1 [23 - 50]	43·0±11·9 [28 - 66]	38·7±11·3 [24 - 57]	HC < UA (p=0·0152) HC = KS UA = KS
Fagerstrom[b]	0·6±1·5 [0-6]	4·4±3·5 [0 - 14]	4·0±4·0 [0 - 10]	HC < UA (p=0·0002) HC = KS UA = KS
CLINICAL DATA				
Abstinence before inclusion (days)	N/A	11·4±5·0 [4 - 24]	N/A	
Alcohol Use (years)	N/A	31·3±9·4 [18 - 51]	N/A	
Alcohol misuse (years)	N/A	19·7±9·1 [2 - 34]	N/A	
Alcohol dependence (years)	N/A	9·9±8·1 [1 - 34]	N/A	
Alcohol consumption over last 30 days	N/A	20·0±9·0 [0 - 40]	N/A	
Number of previous detoxifications	N/A	2·5±2·4 [0 - 11]	N/A	
NEUROPSYCHOLOGICAL DATA				
Global cognitive evaluation				
Mini Mental State (MMS) (/30)	28·6±1·1 [27 - 30]	27·1±2·7 [20 - 30]	23·6±2·6 [18 – 27]	HC > KS (p=0·0001) UA > KS (p=0·0003)
MATTIS Total score	141±2·0 [136 - 144]	135± 8·5 [107 - 143]	120±9·9 [95-133]	HC > UA (p=0·0254) HC > KS (p=0·0001) UA > KS (p=0·0001)
Verbal episodic memory				
FSCRT: sum of 3 free recalls	33·6±4·9	28·1±8·6	5·9±2·9	HC > UA (p=0·0403) HC > KS (p=0·0001) UA > KS (p=0·0001)
CVLT: sum of 5 immediate recalls				HC = UA (p=0·0877) HC > KS (p=0·0001) UA > KS (p=0·0001)
Executive functions				
MCST: number of perseverative responses	0·95±1·2	2·8±3·4	5·4±4·7	HC = UA HC < KS (p=0·0079) UA = KS

HC = Healthy Controls; UA = Uncomplicated Alcoholics; KS = Alcoholics with Korsakoff's Syndrome
Mean ± standard deviation and range [minimum – maximum] are reported.
* : ANCOVA with age and gender as covariate F(2,57);
§ : ANCOVA with gender as covariate F(2,58);
Post-hoc HSD Tukey for unequal sample sizes (p-values shown for when p<0·05)

FSCRT: Free and Cued Selective Reminding Test; MCST: Modified Card Sorting Test
a : State-Trait Anxienty Inventory for adults , Y-A for “state anxiety” and Y-B for “trait anxiety”
b : Fagerstrom
Note: Alcohol drinking history data for KS patients could either not be obtained or their accuracy could not be verified.